Multidimensional Diagnostics of Turbine Cavitation[1]

B. Bajic
Managing Director,
Korto Cavitation Services–Korto GmbH,
12, rue Ste Zithe
L-2763 Luxembourg, Luxembourg
e-mail: korto@cavitation.de

A novel technique for vibro-acoustical diagnostics of turbine cavitation is introduced and its use demonstrated on a Francis turbine. The technique enables identification of different cavitation mechanisms functioning in a turbine and delivers detailed turbine cavitation characteristics, for each of the mechanisms or for the total cavitation. The characteristics specify the contribution of every critical turbine part to the cavitation intensity. Typical diagnostic results: (1) enable optimization of turbine operation with respect to cavitation erosion; (2) show how a turbine's cavitation behavior can be improved; and (3) form the basis for setting up a high-sensitivity, reliable cavitation monitoring system. [DOI: 10.1115/1.1511162]

Introduction

In a long list of recent publications on the methods of vibro-acoustical diagnostics of hydro turbine cavitation ([1–20]), little can be found regarding the problem of identifying turbine parts that cause cavitation. This seems to be the consequence of the fact that most measurements have been performed with *one sensor* using *mean values* of vibro-acoustical signatures. While such measurements can possibly yield an overall description of cavitation performance of a turbine, they can hardly furnish any details as to the cause of cavitation. In order to distinguish between different cavitating elements of a turbine, spatial resolution is needed. Because the space-time configuration of the acoustical field in a turbine is unsuitable for coherent acoustical measurements that might result in directivity or focusing on a source, one has to try incoherent processing based on parametric differences produced by the inhomogeneity of a transfer function or source structure. In one such approach, introduced in Bajic [9] and elaborated in Bajic [16], one analyzes the dependence of cavitation noise power on the instantaneous angular position of a turbine runner. In case of weak or moderate cavitation this yields data that enable estimation of contributions of various pairs of stator/runner blades to the total cavitation intensity. Fundamentally, this method is based on using an *additional dimension* of data which usually has been ignored and omitted by circumferential averaging. Another case in which one distinguishes between spatially separated segments of a cavitating flow and identifies contributions arising from different runner blades has been reported in Hermann et al. [18]. However, the method is not described by the reference.

In this paper an approach to vibro-acoustical diagnostics of turbine cavitation is presented that systematically uses the *multidimensionality* of vibro-acoustical signatures of cavitation in order to infer details of cavitation in a turbine. A number of spatially separated sensors are utilized to pick up differences in the dependence of cavitation on the runner's angular position, and these data are studied as a function of noise frequency and turbine power. By using the resolution in a combination of dimensions—sensors' location, noise frequency, runner's instantaneous angular position, turbine power—it is possible to distinguish between different cavitation mechanisms and their causes (i.e., different turbine parts that cause cavitation), and to quantify their respective contributions to cavitation intensity. As concluded in a critique of the present practice of the vibro-acoustical cavitation diagnostics (Bajic [20]) such an approach has to be truly multidimensional and not a simple series of analyses in which only one independent element is varied in each step.

Experiment

The multidimensional measurement and analysis procedure was verified by means of the data collected on a 17 MW, double-runner, horizontal-axis Francis turbine in which 19 runner blades are rotating behind 20 guide vanes. On the shaft of each guide vane a high-frequency vibro-acoustical sensor was fixed (Fig. 1). The instantaneous angular position of the runner, described by the angle θ (increasing in the direction of rotation and being zero when the reference blade is in the reference position), was controlled. 100 signal samples, each covering one revolution period, were recorded at each sensor and in every operating condition of the turbine. The signal recording was synchronized with runner rotation, and the 100 samples were used to produce deterministic descriptors of random cavitation noise signals by averaging over 100 revolutions. The frequency range from the revolution frequency up to 1 MHz was covered. More than 40 gigabytes of vibro-acoustical data were collected and analyzed. The steps of the analysis are presented in what follows.

Experimental Data

The power density spectra of noise recorded by means of the sensor at the guide vane $v = 1$ are illustrated in Fig. 2. The spectra measured at the other guide vanes were similar. In a broad frequency range between 0.2 kHz and 1 MHz there is a noticeable dependence on turbine power. Narrow peaks at frequencies above 10 kHz are due to sensor resonances and vibro-acoustic resonances of the turbine.

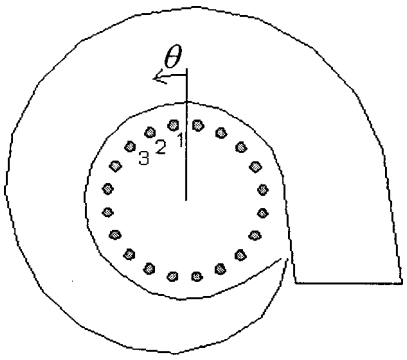

Fig. 1 The sensors placed on the 20 guide vanes react to cavitation in various locations around the spiral

[1]Presented at the Hydraulic Machinery and Systems—20th IAHR Symposium, Aug. 6–9, 2000, Charlotte, NC.

Contributed by the Fluids Engineering Division for publication in the JOURNAL OF FLUIDS ENGINEERING. Manuscript received by the Fluids Engineering Division December 1, 2000; revised manuscript received May 6, 2002. Associate Editor: Y. Tsujimoto.

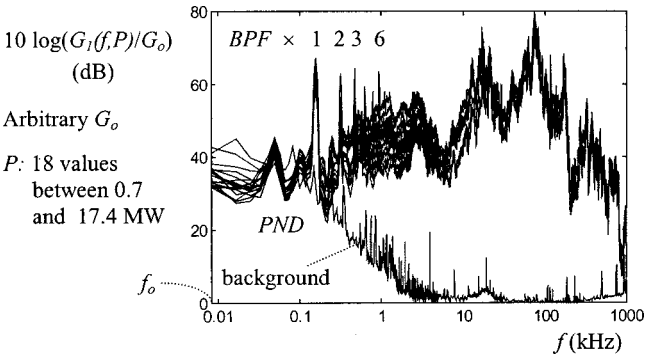

Fig. 2 Typical power density spectra of noise picked up at different power values. There is no noticeable line at the revolution frequency, but the blade-passage frequency (BPF) lines are rather strong. The background noise, recorded in the turbine at rest while the other machinery in the plant was operating, is low enough to enable reliable estimation of the continuous spectrum component between 0.3 and 800 kHz.

In another format, as normalized spectra (Bajic and Keller [6]) the data from Fig. 2 are shown in Fig. 3. Most resonance peaks, other traces of transfer functions, and the BPF-harmonics disappear. Free from these cavitation-irrelevant issues, such spectra illuminate the influence of turbine load on cavitation in a more objective way. They also may reveal cavitation details hardly visible in nonnormalized spectra.

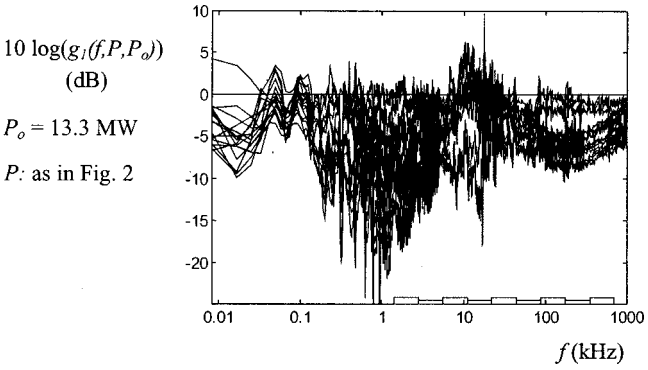

Fig. 3 Overview of the normalized power spectra. The $v=1$ power density spectra recorded at different turbine power values are compared to the one recorded at 13.3 MW. The spectrum related to this reference value is thus represented by the zero-dB line.

The dependence of noise intensity on the angular position of the runner found in the measurements is illustrated by the polar diagrams in Fig. 4. These were obtained by means of the sensor at $v=1$. Similar, but not identical, patterns were recorded at the other guide vanes.

Identification of Cavitation Mechanisms

A two-dimensional representation of the $v=1$ normalized spectra presented in Fig. 5 yields both detailed and overall insight into the structure of data in the (f, P)-domain. Although the information content of the data in Fig. 3 and Fig. 5 is identical, much more can be inferred from Fig. 5. First of all, two dominant patterns can be recognized in the body presented by the two views in Fig. 5. These are drawn in Figs. 6(*a*) and 6(*b*) and are interpreted as the vibro-acoustical signatures of two segments of cavitating flow, i.e., *cavitation mechanisms*. With reference to strongly differing spectra, these mechanisms may be assumed hydraulically independent and thus their respective noise power components additive. After subtracting the two components from the total spectrum of Fig. 5, the third mechanism, presented in Fig. 6(*c*), is identified. In this way a useful decomposition of the total spectrum follows:

$$g_v(f,P,P_o)=\sum_{m=0}^{M} {}^{(m)}g_v(g,P,P_o),$$

$M=3$, $v=1$. Here a possibly existing background component, ${}^{(0)}g_v(f,P,P_o)$, is included to enable the most general description. In the present $v=1$ case such a component was not necessary.

Estimates of cavitation intensity based on noise power measured within a limited frequency band are highly biased due to strong differences in the forms of the spectra of the three mechanisms. In order to suppress this error, the total noise power, $I_v(P)$, should be used as an estimate of cavitation intensity and not an arbitrary part of it (Bajic [16]). This also holds true for the estimates of the cavitation intensity of cavitation mechanisms, ${}^{(m)}I_v(P)$. These follow from the normalized spectra, ${}^{(m)}g_v(f,P,P_o)$, identified by the empirical procedure illustrated above:

$${}^{(m)}G_v(f,P)={}^{(m)}g_v(f,P,P_o)\times G_v(f,P_o),$$

$${}^{(m)}I_v(P)=\int_0^{\infty} {}^{(m)}G_v(f,P)df,$$

and thus

$$I_v(P)=\sum_{m=0}^{M} {}^{(m)}I_v(P).$$

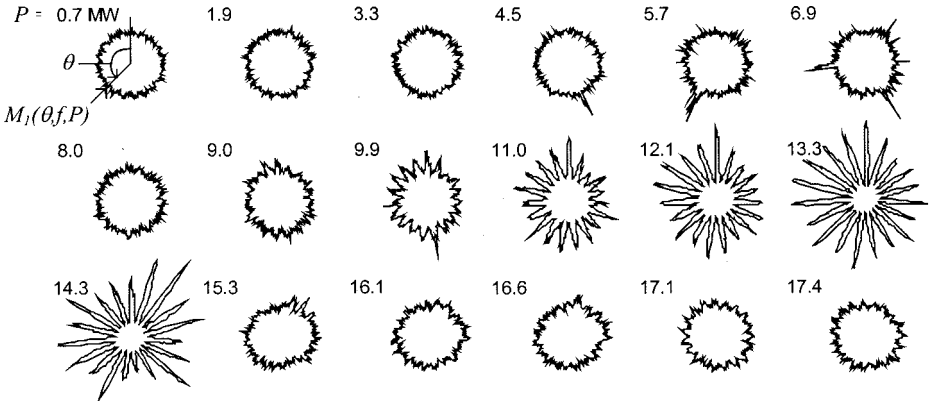

Fig. 4 An example of modulation curves: $M_1(\theta,f,P)$ in an octave band centered at $f=125$ kHz measured at different turbine power values

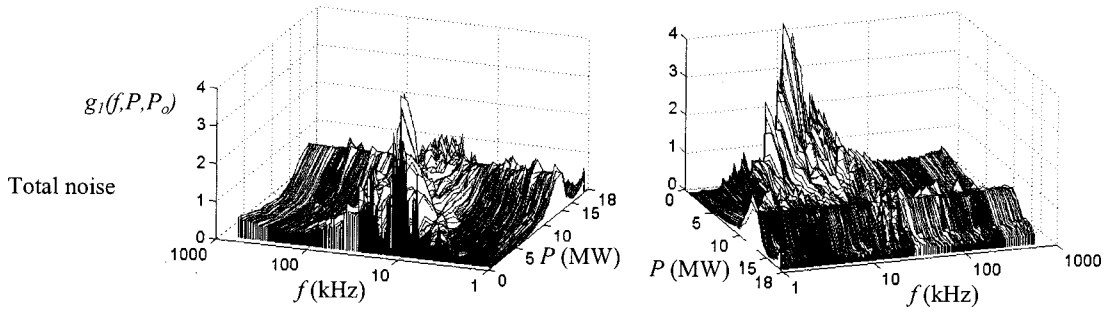

Fig. 5 Normalized spectra of Fig. 3 (P_o=13.3 MW) presented two dimensionally, seen from two perspectives

This last form of the cavitation description, in which there is no longer frequency dependence, will be used as a final cavitation intensity estimate. As to the turbine-power dependence of the relative intensities of the mechanisms, it will be assumed that its form stays the same for all the frequency components contributing to a particular mechanism. Consequently, the dependence found within a narrow frequency range that is typical for the mechanism (Fig. 7) will be used:

$m=1$: octave band centered at $f=31.5$ kHz, $0<P$ (MW)<7;
$m=2$: octave band centered at $f=125$ kHz, $7<P$ (MW)<14;
$m=3$: octave band centered at $f=125$ kHz, $14<P$ (MW).

Cavitation Intensity Estimates

A weak point in the previous discussion derives from the fact that everything in it is based on the results obtained on only one guide vane, $v=1$. While such results may rather safely be used to identify the $(f,P)_m$ ranges and to optimize the analysis, no quantitative estimates of cavitation intensity may be derived from them. Indeed, as stated in Bajic [20], spatial averaging is necessary to derive stable estimates of cavitation intensity which would be representative of all the segments of a cavitating flow. Thus, instead of $I_v(P)$ and ${}^{(m)}I_v(P)$, the estimates

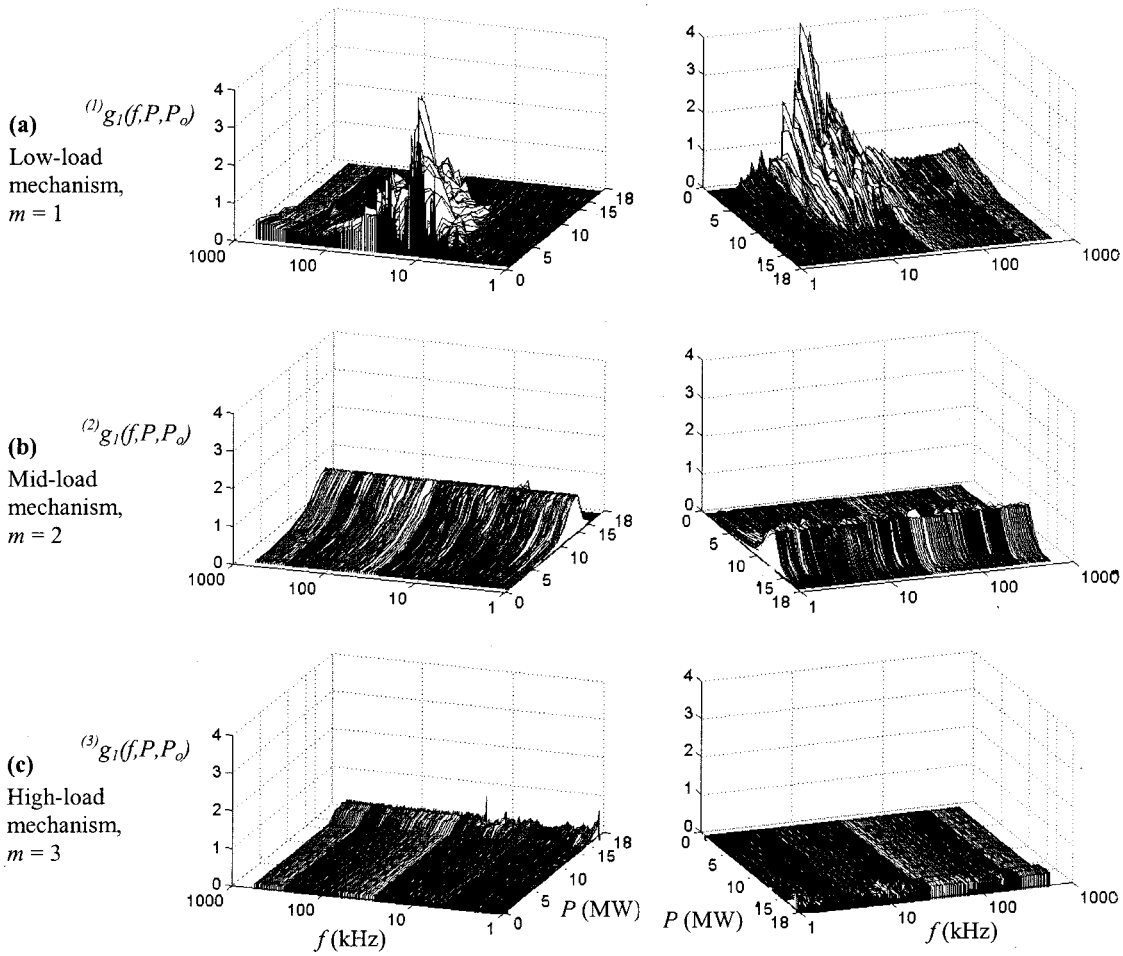

Fig. 6 Noise decomposition: contribution of the three cavitation mechanisms to the total noise

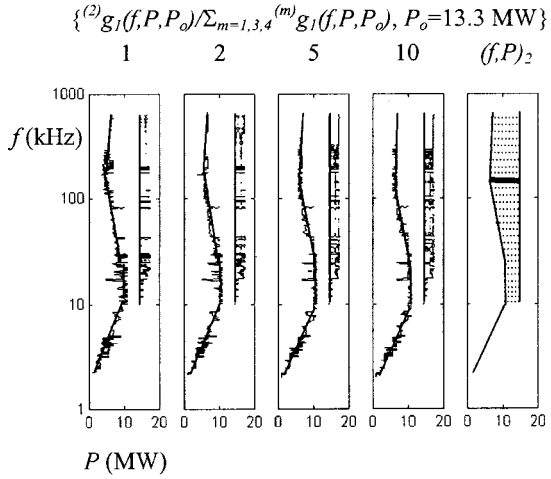

Fig. 7 The way used to determine the range of prevalence of a mechanism m, $(f,P)_m$, in the total noise is illustrated here by the $m=2$ case. At the P-values between the pairs of curves the $m=2$ intensity is equal resp. 2, 5, or 10 times stronger than the rest of the intensity. There from the $(f,P)_2$ denoted; the ratio 5 is assumed sufficiently high.

$$I(P)=\langle I_v(P)\rangle_v \quad \text{and} \quad {}^{(m)}I(P)=\langle {}^{(m)}I_v(P)\rangle_v$$

should be used. One more calibration step is needed in order to produce a stable and representative estimate of the total cavitation intensity, $C(P)$. The data related to the chosen frequency bands that are found suitable for the estimation of the mechanisms should be combined into the estimates of the mechanisms' intensities. This can be done by making the contribution to the cavitation intensity of the mechanism m, ${}^{(m)}C(P)$, stemming from the vane v, proportional to the quantity

$$\frac{G_v(f,P)}{G_1(f,P)}\times {}^{(m)}I_1(P), \quad (f,P)\in(f,P)m,$$

where stable-in-f low-resolution spectra should be used. Such data, which are based on the total noise power but incorporate the dependence on turbine power as it is described by the spectra determined within the (f, P) ranges specific for the mechanism considered, are then averaged over all the v's to yield the final estimates of the mechanisms' intensity. Considered within their respective (f, P) ranges and summed, these estimates then yield the final estimate of the total cavitation intensity. Additionally, this final estimate—which is not more than a relative estimate of cavitation intensity—is normalized relative to its maximum.

Role of Guide Vanes and Runner Blades

The 19 equidistant peaks in the modulation curves of Fig. 4, noticeable at most power values but strongest between 9.9 and 14.3 MW, are due to interaction of one guide vane (in this case $v=1$) and the 19 runner blades. Such modulation curves obtained at all the guide vanes, in the same frequency band as in Fig. 4 at a power value lying within $(f,P)_2$, are presented in Fig. 8(b). This strong BPF-modulation is found to be characteristic of mechanism 2. As to mechanism 1, the modulation in its (f, P) range, illustrated by the 1.9 MW curve in Fig. 8(a), is undetectable. The small fluctuations observable there are due to random errors. The situations like these in Figs. 8(a) and 8(b) were found within the whole $(f,P)_1$ and $(f,P)_2$ ranges. Therefore, as to the mechanisms 1 and 2, the noise produced by mechanism 1 does not depend on the angular position of the runner, and there is a series of 19 peaks for every guide vane in the modulation curves of noise produced by mechanism 2.

An interesting regularity can be noted in the set of 19×20 peaks related to mechanism 2. There is a systematic shift of the

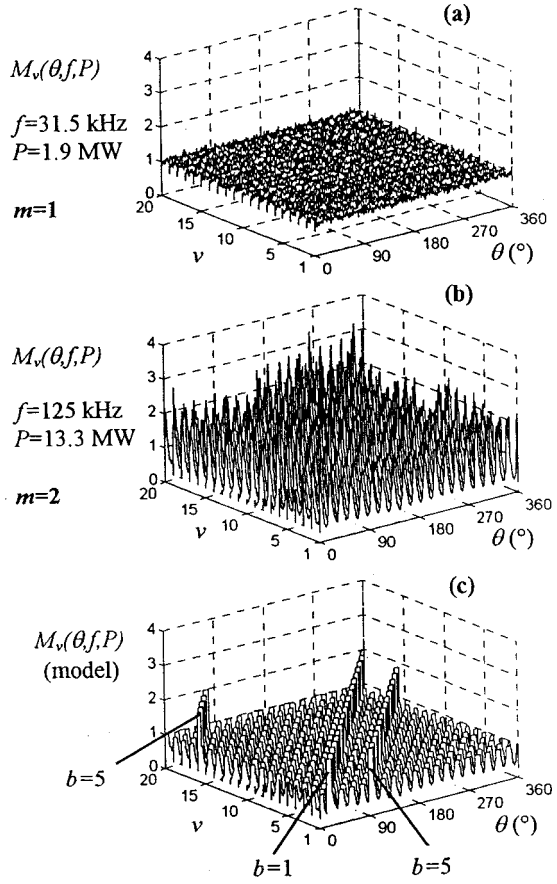

Fig. 8 Typical cases of noise modulation

peaks related to the same runner blade as detected by the subsequent guide vanes. This is illustrated in Fig. 8(c) by the model which was derived by manipulating the amplitudes of the peaks of Fig. 8(b) while leaving their positions unchanged. As an example, two series of peaks are denoted here, the ones due to the interaction of runner blades 1 and 5 with the 20 guide vanes. Obviously, the regularity found in the modulation waveforms can be used to identify the contribution of each runner blade to the noise measured at every guide vane. Here the assumption has to be introduced that a distinct maximum related to a particular b/v-pair stems from cavitation in the vicinity of the guide vane v and thus can be used as a measure of its cavitation activity. Such a heuristic assumption is supported by the form of the peaks and the fact that they do not overlap (cf. Figs. 4 and 8(b)).

A filtering procedure based on the regularity of the described $M_v(\theta,f,P)$ structure has been devised and applied to the modulation data. Allowing for a small random spread of angular positions of the peaks, the peaks' maxima were estimated. These were attributed to the related v's and b's and denoted by $M_v^b(f,P)$. Such data were then classified with respect to the f and P values, so that the estimates, ${}^{(m)}M_v^b(P)$, of the component generated by the mechanisms were derived. These were defined by

$${}^{(m)}M_v^b(P)=M_v^b(f,P)|_{(f,P)\in(f,P)_m}$$

because there were no significant variations of $M_v^b(f,P)$ within $(f,P)_m$. An alternative for the opposite case reads

$${}^{(m)}M_v^b(P)=\langle M_v^b(f,P)|_{(f,P)\in(f,P)_m}\rangle_f.$$

Note that there are only four variables in these estimates: m, v, b, and P; noise frequency has disappeared.

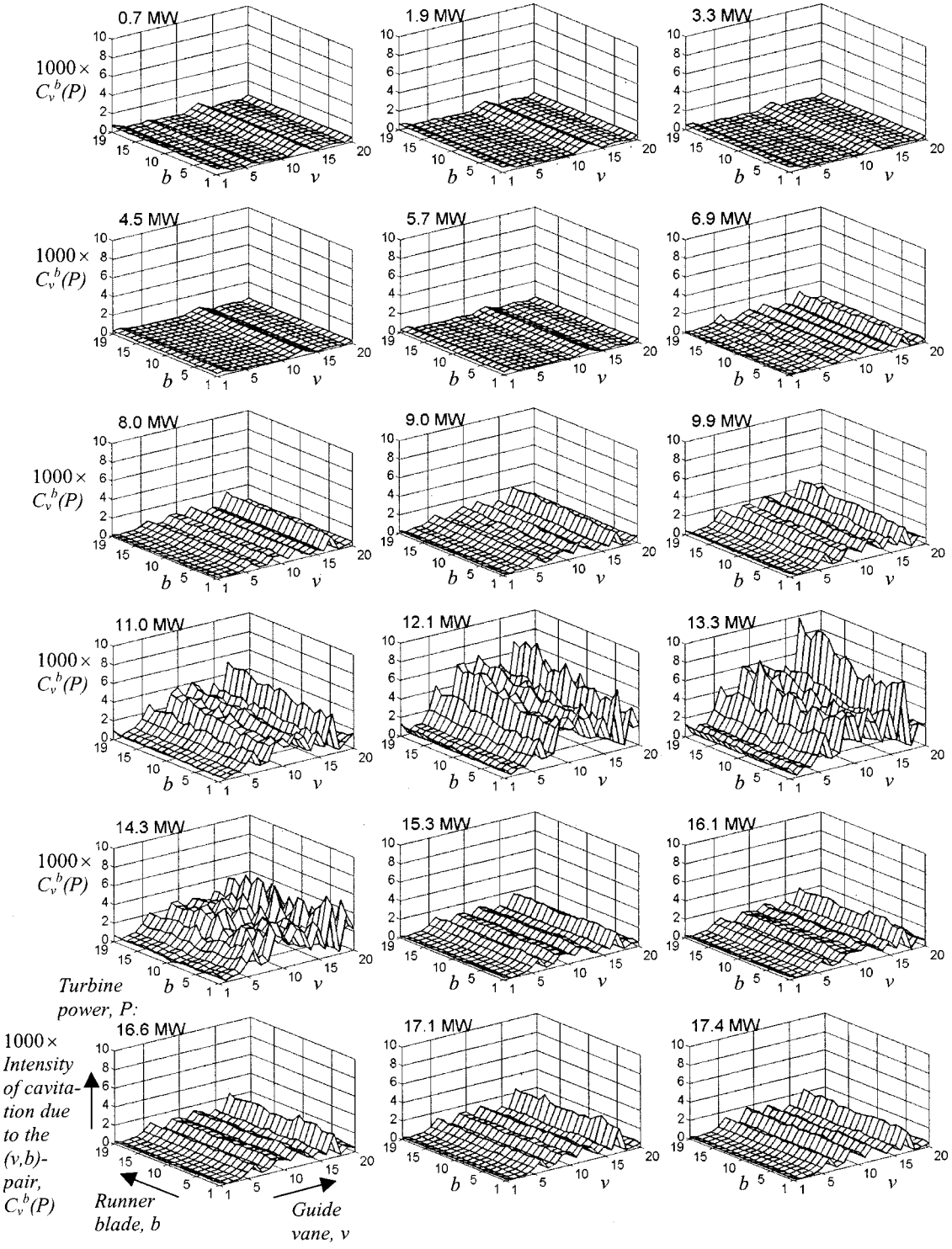

Fig. 9 The fine-structure cavitation characteristics of the turbine: the most detailed description of cavitation that can be obtained by the multidimensional method. For each tested turbine-power value, *P*, there are 380 (number-of-runner-blades×number-of-guide-vanes) dimensionless values, C_v^b, that stand for the intensity of cavitation caused by the interaction of a pair consisting of the runner blade *b*, and the guide vane *v*. The C_v^b-values specify the relative intensity of cavitation. Their use in cavitation erosion estimation is discussed elsewhere (Bajic [14,17]). The data presented in the figure describe total cavitation. The method also enables identification of different segments of a cavitating flow—cavitation mechanisms—and yields data like this for each of them.

In order to transform these results of modulation analysis into the estimates of true intensities like those presented in Fig. 9, the quantities

$$ {}^{(m)}I_v^b(P) = {}^{(m)}I_v(P)\left[{}^{(m)}M_v^b(P) \Big/ \sum_{b'=1}^{B} {}^{(m)}M_v^{b'}(P) \right]$$

were computed and used in the following formulas:

$$ {}^{(m)}C_v^b(P) = k\,{}^{(m)}I_v^b(P), \quad C_v^b(P) = \sum_{m=1}^{M} {}^{(m)}C_v^b(P), $$

$$ {}^{(m)}C^b(P) = \sum_{v=1}^{V} {}^{(m)}C_v^b(P), \quad C^b(P) = \sum_{v=1}^{V} C_v^b(P), $$

$$ {}^{(m)}C_v(P) = \sum_{b=1}^{B} {}^{(m)}C_v^b(P), \quad C_v(P) = \sum_{b=1}^{B} C_v^b(P), $$

$$ {}^{(m)}C(P) = \sum_{b=1}^{B}\sum_{v=1}^{V} {}^{(m)}C_v^b(P), \quad C(P) = \sum_{b=1}^{B}\sum_{v=1}^{V} C_v^b(P); $$

by means of the calibration constant

$$ k = \left[\max_P \sum_{m=1}^{M}\sum_{b=1}^{B}\sum_{v=1}^{V} {}^{(m)}I_v^b(P) \right]^{-1}. $$

$C(P)$ was scaled to a maximum value of 1.

Turbine Cavitation Characteristics

The C-functions of turbine power, P, introduced above, are turbine cavitation characteristics. Four of them deal with all the cavitation mechanisms at once and differ only in the degree and type of resolution with respect to turbine parts—guide vanes, v, and runner blades, b:

$C_v^b(P)$ *fine-structure characteristic*,
$C^b(P)$ *runner characteristic*,
$C_v(P)$ *wicket gate characteristic*, and
$C(P)$ *global turbine characteristic*.

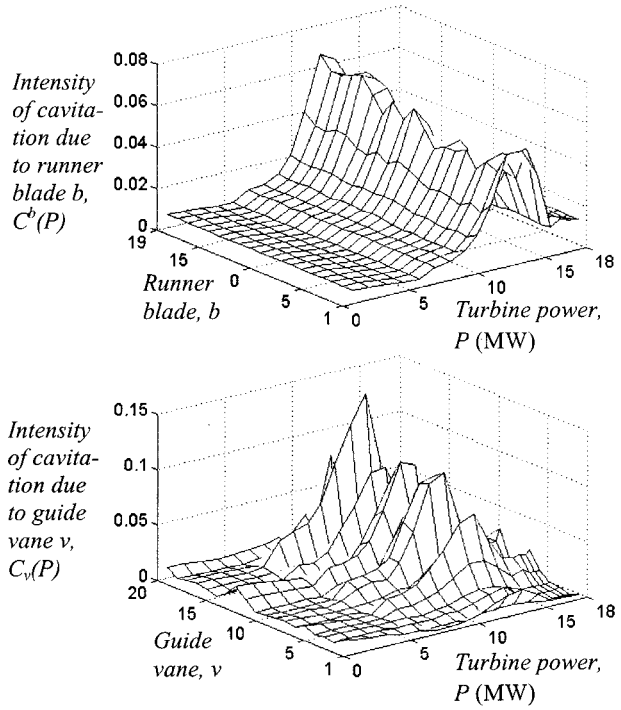

Fig. 10 Runner and wicket gate cavitation characteristics

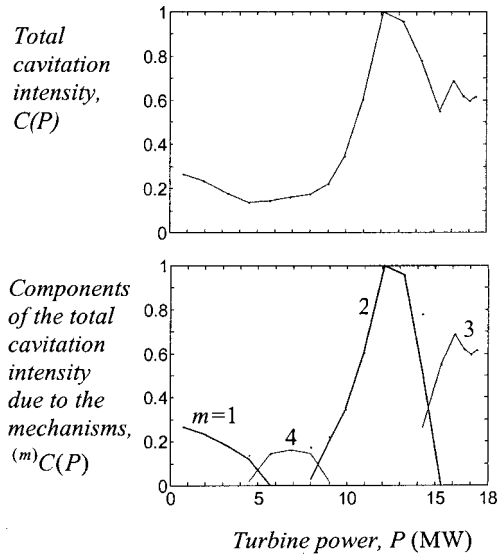

Fig. 11 Global turbine characteristics without and with resolution with respect to cavitation mechanisms

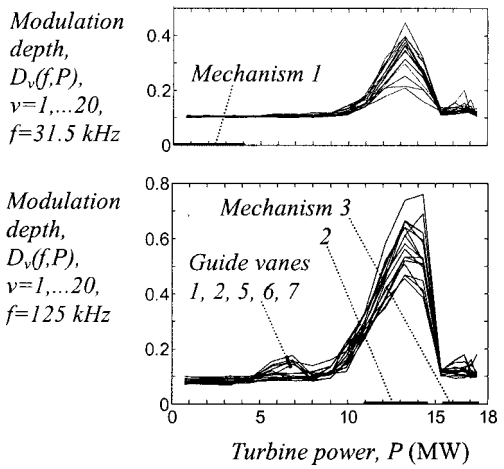

Fig. 12 Check of (in)stationarity: variation of cavitation intensity at the (f,P)-values characteristic of the mechanisms

The other four (sets of) characteristics, ${}^{(m)}C_v^b(P)$, ${}^{(m)}C^b(P)$, ${}^{(m)}C_v(P)$, and ${}^{(m)}C(P)$, yield the same description of cavitation as above but separately for every one of M mechanisms, $m = 1, \ldots M$. Some of the characteristics derived for the turbine considered are illustrated in Figs. 9–11.

Conclusion

Vibro-acoustical diagnostics of turbine cavitation based on a number of suitably located sensors and multidimensional data processing, proposed and verified here, utilizes an exhaustive set of measurement data to reconstruct a virtual vibro-acoustic picture of cavitation, which enables iterative adaptive analyses and thus reveals details that otherwise may remain undetected. Such multidimensional diagnostics enables identification of different cavitation mechanisms functioning in a turbine, proves to be a highly sensitive tool for reliable estimation of turbine cavitation characteristics, and yields detailed quantitative descriptions of the role critical turbine parts play in the cavitation process. It removes several disadvantages encountered in practice with simpler approaches.

Typical diagnostic results enable optimizing a turbine's operation with respect to cavitation erosion and improving a turbine's

cavitation behavior if necessary. The results may also be used to set up a high-sensitivity, reliable, application-specific cavitation monitoring system.

Acknowledgment

The experimental data used in this paper were collected on a turbine of the Walchensee Hydro Powerplant owned by the Bayernwerk Wasserkraft AG, Bavaria, Germany. The author is grateful to Dr. Andreas-Peter Keller of Hydraulic Research Laboratory of the Munich University of Technology in Obernach and Dipl.-Ing. Hans-Peter Schanderl of the Walchensee Hydro Powerplant for initiating and enabling these measurements.

Nomenclature

b = runner blade
B = number of runner blades, $B=19$
BPF = blade-passage frequency, Bf_o
$C(P)$ = total cavitation intensity
$C_v(P)$ = intensity of the cavitation component due to action of guide vane v
$C^b(P)$ = intensity of the cavitation component due to action of runner blade b
$C_v^b(P)$ = intensity of the cavitation component due to action of the (v,b)-pair
${}^{(m)}C(P)$ = intensity of cavitation mechanism m
${}^{(m)}C_v(P)$ = intensity of the component of cavitation mechanism m due to action of guide vane v
${}^{(m)}C^b(P)$ = intensity of the component of cavitation mechanism m due to action of runner blade b
${}^{(m)}C_v^b(P)$ = intensity of the component of cavitation mechanism m due to action of the (v,b)-pair
$D_v(f,P)$ = $\langle [M_v(\theta,f,P)-1]^2\rangle \theta^{1/2}$
= modulation depth
f = noise frequency
f_o = revolution frequency, $f_o=500\ \mathrm{min}^{-1}$
$(f,P)_m$ = part of the (f, P)-domain within which mechanism m is domineering
G_o = reference power-spectrum value
$g_v(f,P,P_o)$ = $G_v(f,P)/G_v(f,P_o)$
= normalized power spectrum
$G_v(f,P)$ = power spectrum density of noise sensed at guide vane v (various resolutions)
${}^{(m)}g_v(f,P,P_o)$ = component of $g_v(f,P,P_o)$ generated by mechanism m
${}^{(m)}G_v(f,P)$ = component of $G_v(f,P)$ generated by mechanism m
I_o = reference noise-power value
$I(P)$ = total noise power
$I_v(P)$ = total noise power as sensed on v
${}^{(m)}I(P)$ = power of noise component generated by mechanism m
${}^{(m)}I_v(P)$ = power of noise component generated by mechanism m as sensed on v
${}^{(m)}I_v^b(P)$ = power of noise component generated by mechanism m due to action of the (v,b)-pair
k = calibration constant
m = cavitation mechanism $(1,2,\ldots M)$; $m=0$ background
M = number of cavitation mechanisms detected in the turbine
$M_v(\theta,f,P)$ = amplitude modulation of noise power sensed at v at power P within a chosen frequency band centered at f, expressed as a function of θ; $\langle M_v(\theta,f,P)\rangle_0=1$
$M_v^b(f,P)$ = peak value (in θ) of the component of $M_v(\theta,f,P)$ related to the (v,b)-pair
${}^{(m)}M_v^b(P)$ = component of $M_v^b(f,P)$ related to mechanism m
P = turbine power
P_o = reference turbine-power value
PND = power net disturbance
v = guide vane (1, 2, 3, . . . in Fig. 1)
V = number of guide vanes, $V\approx 20$
θ = instantaneous angular position of the runner
$\langle\rangle_f$ = averaging over f within a denoted band
$\langle\rangle_v$ = averaging over $v=1,2,\ldots V$
$\langle\rangle_\theta$ = averaging over $\theta\in[0,2\pi]$

References

[1] Abbot, P. A., 1989, Am. Soc. Mech. Eng., **FED-Vol. 88**, pp. 55–61.
[2] Abbot, P. A., and Morton, D. W., 1991, Am. Soc. Mech. Eng., **NCA-Vol. 10**, pp. 75–84.
[3] Gülich, J.-F., 1992, Technische Rundschau Sulzer, (1), pp. 30–35.
[4] Knapp, W., Schneider, Ch., and Schilling, R., 1992, I Mech E, C453/048, pp. 271–275.
[5] Bourdon, P., Simoneau R., and Avellan, F., 1993, Am. Soc. Mech. Eng., **FED-Vol. 176**, pp. 51–67.
[6] Bajic, B., and Keller, A., 1996, ASME J. Fluids Eng., **118**, pp. 756–761.
[7] Farhat, M., Bourdon P., and Lavigne P., 1996, *Conf. Modelling, Testing & Monitoring for Hydro Powerplants II*, Lausanne, Switzerland, pp. 151–160.
[8] Vizmanos, C., Egusquiza, E., and Jou E., 1996, *Conf. Modelling, Testing & Monitoring for Hydro Powerplants II*, Lausanne, Switzerland, pp. 161–168.
[9] Bajic, B., 1996, *Conf. Modelling, Testing & Monitoring for Hydro Powerplants II*, Lausanne, Switzerland, pp. 169–178.
[10] Kaye, M., Holenstein, A., Dupont Ph., and Rettich J., 1996, *Conf. Modelling, Testing & Monitoring for Hydro Powerplants II*, Lausanne, Switzerland, pp. 179–188.
[11] Bourdon, P., Farhat, M., Simoneau, R., Pereira, F., Dupont, Ph., Avellan, F., and Dorey J.-M., 1996, *XVII IAHR Symp. Hydraulic Machinery and Cavitation*, Valencia, Spain, **1**, pp. 534–543.
[12] Dorey, J. M., Laperrousaz, E., Avellan, F., Dupont, Ph., Simoneau, R., and Bourdon, P., 1996, *XVIII IAHR Symp. Hydraulic Machinery and Cavitation*, Valencia, Spain, **1**, pp. 564–573.
[13] Dupont, Ph., Caron, J.-F., Avellan, F., Bourdon, P., Lavigne, P., Farhat, M., Simoneau, R., Dorey, J.-M., Archer, A., Laperrousaz, E., and Couston, M., 1996, *XVIII IAHR Symp. Hydraulic Machinery and Cavitation*, Valencia, Spain, **1**, pp. 574–583.
[14] Bajic, B., 1996, Int. J. Hydropow. Dams, **3**, pp. 45–50; also: Wasserwirtschaft, **88**, 1998, pp. 26–31.
[15] Farhat, M., Bourdon, P., Lavigne, P., and Simoneau, R., 1997, Am. Soc. Mech. Eng., **FEDSM97**, Paper No. 3250.
[16] Bajic, B., 1997, *Conf. Hydropower Into the Next Century*, Portoroz, Slovenia, pp. 185–196.
[17] Bajic, B., 1998, *Third Int. Symp. on Cavitation*, Grenoble, France, **1**, pp. 359–362; also: Wasserwirtschaft, **89**, 1999, pp. 182–186.
[18] Hermann, O., Holenstein, A., Keck, H., and Rettich, J., 1998, *4. Symp. Methoden, Nutzen und Trends der diagnostischen Überwachung von Maschinenschwingungen und weiteren Zustandsgrößen in Wasserkraftanlagen*, Innsburck, Austria, TIWAG-Schenck, pp. 207–223.
[19] Bajic, B., 1998, *Conf. Modelling, Testing & Monitoring for Hydro Powerplants III*, Aix-en-Provence, France, pp. 641–652.
[20] Bajic, B., 1998, *10. Int. Seminar Wasserkraftanlagen*, Vienna, Austria, pp. 447–458.